Anion Ordering, Magnetic Structure and Properties of the vacancy ordered perovskite $Ba_3Fe_3O_7F$

Oliver Clemens, Christian Reitz, Ralf Witte, Robert Kruk, Ronald I. Smith

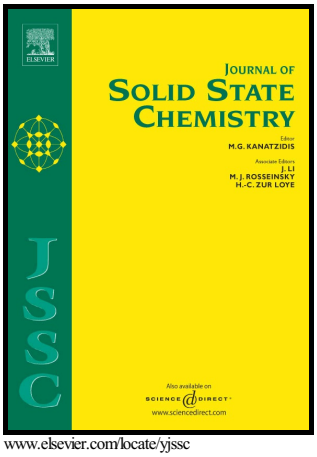

www.elsevier.com/locate/yjssc

PII: S0022-4596(16)30300-0
DOI: http://dx.doi.org/10.1016/j.jssc.2016.07.033
Reference: YJSSC19480

To appear in: *Journal of Solid State Chemistry*

Received date: 13 June 2016
Revised date: 29 July 2016
Accepted date: 31 July 2016

Cite this article as: Oliver Clemens, Christian Reitz, Ralf Witte, Robert Kruk and Ronald I. Smith, Anion Ordering, Magnetic Structure and Properties of the vacancy ordered perovskite $Ba_3Fe_3O_7F$, *Journal of Solid State Chemistry* http://dx.doi.org/10.1016/j.jssc.2016.07.033

Anion Ordering, Magnetic Structure and Properties of the vacancy ordered perovskite $Ba_3Fe_3O_7F$

Oliver Clemens[a,b,c*], Christian Reitz[b], Ralf Witte[b], Robert Kruk[b], Ronald I. Smith[d]

[a]Technische Universität Darmstadt, Joint Research Laboratory Nanomaterials, Jovanka-Bontschits-Straße 2, 64287 Darmstadt, Germany.

[b]Karlsruher Institut für Technologie, Institut für Nanotechnologie, Hermann-von-Helmholtz-Platz 1, 76344 Eggenstein-Leopoldshafen, Germany.

[c]University of Birmingham, School of Chemistry, Birmingham, B15 2TT, United Kingdom.

[d]ISIS Facility, Rutherford Appleton Laboratory, Harwell Oxford, Didcot, OX11 0QX, United Kingdom.

*Corresponding Author: Fax: +49 6151 16 20965, E-Mail: oliver.clemens@nano.tu-darmstadt.de

Abstract

This article describes a detailed investigation of the crystallographic and magnetic structure of perovskite type $Ba_3Fe_3O_7F$ by a combined analysis of X-ray and neutron powder diffraction data. Complete ordering of vacancies within the perovskite lattice could be confirmed. In addition, the structure of the anion sublattice was studied by means of the valence bond method, which suggested partial ordering of the fluoride ions on two of the six crystallographically different anion sites. Moreover, the compound was found to show G-type antiferromagnetic ordering of Fe moments, in

agreement with magnetometric measurements as well as previously recorded ^{57}Fe Mössbauer spectroscopy data.

Keywords

Anion Ordering; Vacancy Ordering; Perovskites; Oxyfluorides; Magnetic Structure

TOC Figure

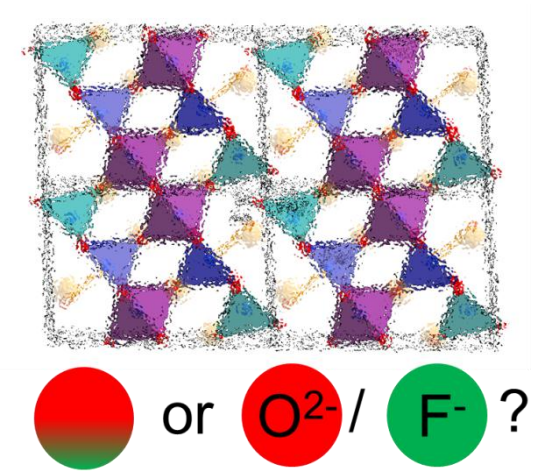

TOC Figure Caption

The vacancy and anion ordered structure of $Ba_3Fe_3O_7F$ is described together with its magnetic properties.

1 Introduction

Oxide and fluoride ions are isoelectronic and have very similar ionic radii, therefore they are found to possess many similar structural and chemical properties [1]. Nevertheless, due to their differing charges ordering between those ions within oxyfluoride compounds is found whenever structures with significantly differing local site potentials can be formed. Apart from materials containing polyanions in addition to fluoride ions (e. g. apatite compounds $A_5(XO_4)_3F$ or other phosphate fluorides), there is a huge variety of compounds which can be prepared by means of high temperature reaction routes known to show ordering between the oxide and fluoride ion [2].

In contrast, ordering between oxide and fluoride ions is not typically encountered for compounds crystallizing within the perovskite type structure. In general, there is only a limited number of perovskite-type oxyfluorides due to the metastable nature of such phases (related to the high stability of alkaline earth fluorides and lanthanide oxyfluorides [3-6]). Therefore, such compounds most often need to be prepared by means of low temperature topochemical reactions. Due to the limited degree of structural reorganisation for topochemical reactions, it is found that ordering between oxide and fluoride ions is most likely to be encountered whenever stacking sequences deviating from a simple *ccp* stacking of the close packed AX_3 layers can be formed (e. g. for Ba-containing perovskites $BaMO_{3-d}F_y$, M = Fe, Co [7-11] with partly *hcp* stacked layers). In this respect, site potentials are significantly different for anions within h-type layers (face shared coordination of M polyhedra) in comparison to anions within c-type layers (corner shared coordination of M polyhedra), which makes ordering of the fluoride (preferential location in h-type layers) and oxide (preferential location in c-type layers) ions energetically favourable.

Detailed investigation of ordering between oxide and fluoride ions from powder diffraction data still remains an experimental challenge. Due to the fact that both ions are isoelectronic and show almost identical scattering lengths for neutrons, they are basically indistinguishable by means of diffraction methods. However, neutron diffraction can facilitate the determination of very precise anion-cation distances, which may then be analysed using the valence bond method [12], enabling the assignment of anions to the different types of crystallographic sites. This method was shown to be a viable tool especially in the case of perovskite type oxyfluoride compounds containing *hcp* stacked layers [7-11] as well as for compounds with K_2NiF_4 or Ruddlesdon-Popper type structures [5, 13].

Among the few oxyfluorides with *ccp* related stacking of AX_3 layers, there is often indication for local, but not necessarily overall ordering of oxide and fluoride ions. When considering the possibility of anion ordering within perovskites one needs to take into account the following factors:

1) Compositions following a formula $A_nB_nO_{3n-i}F_i$ (n, i being integer numbers) must be considered to be a precondition for having *complete* ordering on any distorted perovskite structure being derived from the cubic aristotype (i. e. anion ordering is prohibited per se in the cubic symmetry with space group

Pm-3*m*). Such compositions can be difficult to adjust by means of low temperature fluorination methods, especially for B site cations with good stability with a mixed valent oxidation state. Therefore, for compounds with i being a non-integer number, only partial ordering of anions can be expected.

2) Strong local distortions of polyhedra can arise whenever cations with a strong Jahn Teller effect are contained in a perovskite type structure (being mainly Cu^{2+} or Mn^{3+}). Such compounds possess c/a ratios significantly different from 1, resulting in different site potentials for the anions of an elongated octahedron. However, anion ordering remains questionable even for tetragonally distorted compounds such as $Sr_2Mn_2O_{5-d}F_{1+d}$, with electrostatic energies of mixed and ordered occupations being similar [14].
3) A further driving force for obtaining ordering can result from different A or B site cations being present at the same time, as e. g. found for $Sr_2MnGaO_{5-d}F_{1+d}$ [15, 16], where different anion site potentials are introduced from coordination to different cations. On fluorination of the starting compound Sr_2MnGaO_5 (showing a brownmillerite type structure), fluoride ions were found to be preferably located within the Ga-layers, with the respective crystallographic site being occupied by about 50 % of oxide ions due to reasons of stoichiometry.
4) For compounds with more precisely defined compositions and without strong Jahn Teller type cations (e. g. $BaFeO_2F$ [17-19], $SrFeO_2F$ [20-25], $PbFeO_2F$ [26], $KTiO_2F$ [27], $NaNbO_2F$ [28], $KNbO_2F$ [28]), only small structural distortions are usually encountered with little to no indication for long range ordering of anions. $BaFeO_2F$, $PbFeO_2F$, $KNbO_2F$ and $KTiO_2F$ crystallize in the ideal cubic perovskite structure, with cis- and trans- coordination of the fluoride ions and no indication of anion ordering. For $NaNbO_2F$ and $SrFeO_2F$, orthorhombic structures ($GdFeO_3$ type structure for $NaNbO_2F$ (*Pnma*), *Imma* for $SrFeO_2F$) are found with splitting of the anion site to sites having the correct multiplicity ratio. However, in both cases it is questionable if the distortion arises from anion ordering or simple octahedral tilting to decrease the coordination number of the A-site cation.

Apart from Jahn Teller type distortions or compounds with ns^2 cations, large structural distortions can arise within a *ccp* stacked perovskite type structure whenever deviations from the ideal stoichiometry according to $A_nB_nO_{3n-a}\square_a$ (n, a being

integer numbers) result in reduced symmetry due to ordering of anion vacancies [29]. Therefore, combining a precise fluoride ion composition with a precise vacancy concentration might lead to compounds of the type $A_nB_nO_{3n-i-a}F_i\square_a$ (n, a, i being integer numbers, □ = vacancy). Recently, we found that a compound with composition $Ba_3Fe_3O_7F$ [30] can be formed by low temperature fluorination of $Ba_2Fe_2O_5$ [31-33] using polyvinylidene difluoride (PVDF), which is suitable for precisely adjusting fluorine contents. $Ba_3Fe_3O_7F$ was shown to be vacancy ordered with the presence of only Fe^{3+} from the analysis of laboratory XRD data together with ^{57}Fe Mössbauer spectroscopy [30]. However, determination of the precise anion substructure is difficult when relying on XRD data only. Here we report on a detailed investigation of the crystallographic structure of $Ba_3Fe_3O_7F$ with special focus on the anion sublattice by means of a combined analysis of powder neutron and X-ray diffraction data. This analysis indicates that $Ba_3Fe_3O_7F$ indeed shows full ordering of anion vacancies and must be considered to be at least partially anion ordered, with the fluoride ions being only distributed over two of the six crystallographic anion sites. We furthermore present a detailed description of the magnetic structure and properties of the compound, showing that $Ba_3Fe_3O_7F$ is a G-type antiferromagnet at ambient temperature.

2 Experimental

2.1 Sample preparation

A compound of composition $BaFeO_{3-y}F_{1/3}$ ($Ba_3Fe_3O_{9-y'}F$) was prepared by mixing stoichiometric amounts of $Ba_2Fe_2O_5$ with polyvinylidene difluoride, PVDF (Aldrich). The mixture was thoroughly ground with mortar and pestle in acetone. Initial heating was carried out in air by slowly heating the sample to 370 °C and keeping it at this temperature for 12 h followed by quick cooling.

To obtain a defined oxygen content such as $BaFeO_{7/3}F_{1/3}$ ($Ba_3Fe_3O_7F$) containing trivalent iron only, the as prepared sample was then heated to 450 °C for 24 h inflowing argon (1 SLM, purity 99.998 %), followed by slow cooling to ambient temperature over 2 days.

2.2 X-ray diffraction experiments

The X-ray powder diffraction (XRD) pattern was recorded at ambient temperature on a Bruker D8 diffractometer with Bragg-Brentano geometry and a fine focus X-ray tube with Cu anode. A VANTEC detector and a variable divergence slit (4 mm), with measurement times of 16 h for the angular range of 5 -130 ° 2θ, was used.

Time of flight powder neutron diffraction (NPD) data were recorded at ambient temperature on the GEM diffractometer at the ISIS pulsed spallation source (Rutherford Appleton Laboratory, UK). ~ 1.5 g of powdered $Ba_3Fe_3O_7F$ was loaded into a 6 mm diameter thin-walled, cylindrical vanadium sample can and data collected at ambient temperature for 300 μAh proton beam current to the ISIS target, corresponding to ~ 2 hours exposure in the neutron beam.

2.3 Structural analysis

Coupled analysis of powder diffraction data was performed by using the program TOPAS Academic V5 [34, 35]. The instrumental resolution function for the X-ray data was determined empirically from a set of fundamental parameters [36], using a reference scan of LaB_6 (NIST 660a), and the microstructural parameters were refined to fit the peak shapes for the XRD data. Reflection broadening of the neutron diffraction data was modelled empirically. Full details on the analysis and determination of the crystallographic and magnetic structures will be provided in the respective sections.

2.4 Magnetometric measurements

DC susceptibility measurements were performed over the temperature range 5 - 390 K using a Quantum Design MPMS3 SQUID magnetometer. The sample was pre-cooled to 5 K in zero magnetic field, then a magnetic field $\mu_0 H$ of 50 mT was applied. The susceptibility was subsequently measured whilst warming the sample up to 400 K (ZFC) and then cooling it again in the same magnetic field to 5 K (FC). Field-dependent DC susceptibility measurements were performed on the same instrument at 300 K and 5 K between 0 and 7 T.

3 Results and Discussion

3.1 Analysis of crystallographic structure

In our previous article [30], a model describing the most likely arrangement of anion vacancies was already determined by means of laboratory quality XRD data and the use of group subgroup relationships. In this respect, a variety of monoclinic structures with slightly different space groups were already tested, and indicated a best fit for the structural model with space group $P2_1/m$. As outlined in our preceeding article [30], structural solutions within $P2/m$ could not be ruled out entirely, since intensities of superstructure reflections mainly arise from vacancy ordering within the sublattice of the anions which are weak scatterers in XRD.

This analysis was therefore repeated on the new data set taking into account the additional neutron diffraction data. The quality of fit not only confirmed as correct the previously assigned $P2_1/m$ space group and anion vacancy pattern, but also ruled out the alternative $P2/m$ structural model. This is also in agreement with the simple observation that the (0 1 0) reflection is present neither in the NPD nor in the XRPD data, serving as a further indication for the validity of the presence of the 2_1 screw axis. The final combined analysis of detector banks 2-6 of the GEM TOF diffractometer together with the XRD data is shown in Figure 1 (taking also into account the magnetic scattering, see section 3.2). Apart from monoclinic $Ba_3Fe_3O_7F$ ($P2_1/m$), a very small amount of cubic $BaFeO_{2+x}F_{1-2x}$ ($Pm\text{-}3m$) was found (~ 3 wt-%), which was included into the refinement model (relative amounts of $Ba_3Fe_3O_7F$ and $BaFeO_{2+x}F_{1-2x}$ were constrained to be the same for XRD and NPD data). Structural data are provided in Table 1 with the structure being depicted in Figure 2.

As outlined in the introduction, neutron diffraction is a very powerful tool for determining the detailed structure of the anion sublattice. Assignment of the anions to oxide and fluoride ions will be done later in this section from the analysis of different models by means of the valence bond method, but has already been included in Table 1. However, the valence bond method purely relies on the evaluation of bond distances, and is an *a posteriori* method. Therefore, the labels X1-X6 will be used in the following when discussing the structure of the anion sublattice, recognizing that oxide and fluoride ions have very similar scattering lengths / atomic form factors for the diffraction methods used.

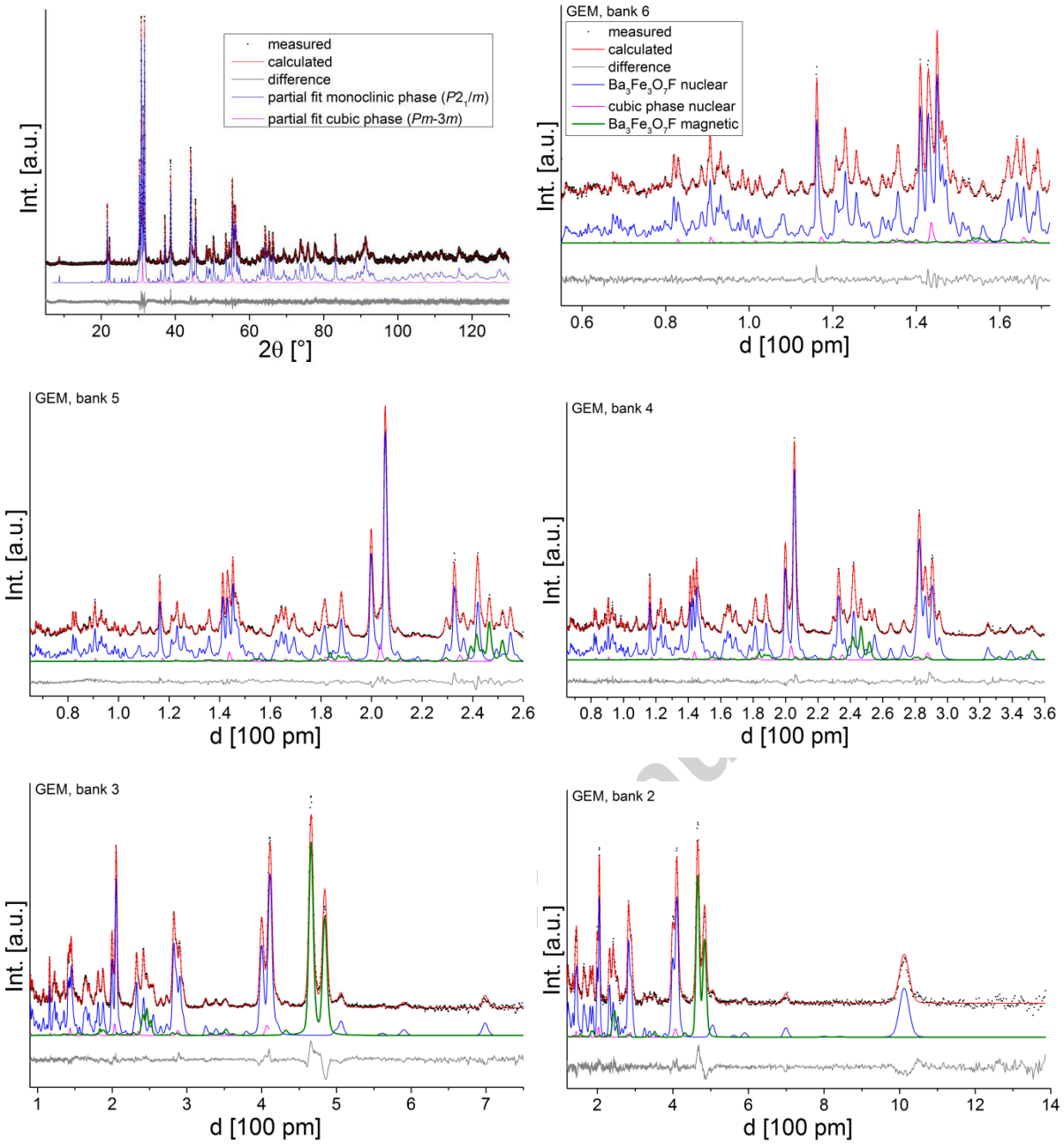

Figure 1. Combined Rietveld analysis of XRPD and NPD data recorded on the sample with composition $Ba_3Fe_3O_7F$. Partial fit curves are shown for nuclear phases (monoclinic $Ba_3Fe_3O_7F$ and cubic $BaFeO_{2+x}F_{1-2x}$) as well as for the magnetic scattering observed from $Ba_3Fe_3O_7F$ (see section 3.2). IN all the patterns shown, the fitted background scattering has been subtracted.

Table 1. Refined crystal structure of $Ba_3Fe_3O_7F$ from a combined analysis of XRPD and NPD data (space group $P2_1/m$).

site label	atom type	Wyckoff site	x	y	z	occ.	B_{iso} [Å^2]
Ba1	Ba^{2+}	2*e*	0.2650(2)	¼	-0.0189(3)	1	0.49(4)
Ba2	Ba^{2+}	2*e*	0.9167(2)	¼	0.7093(2)	1	0.58(4)
Ba3	Ba^{2+}	2*e*	0.5740(2)	¼	0.3427(3)	1	0.26(4)
Fe1	Fe^{3+}	2*e*	0.2636(3)	¼	0.4952(4)	1	1.39(5)
Fe2	Fe^{3+}	2*e*	0.8808(2)	¼	0.2233(3)	1	0.70(5)
Fe3	Fe^{3+}	2*e*	0.6003(3)	¼	0.8287(4)	1	1.04(5)
X1a	O^{2-}	2*e*	0.756(5)	¼	0.008(9)	0.4(2)	0.28(10)
X1b	O^{2-}	2*e*	0.740(4)	¼	0.031(5)	0.6(2)	0.28(10)
X2	O^{2-} / F^-	2*b*	½	***0***	***0***	1	0.80(9)
X3	O^{2-}	2*e*	0.4240(5)	¼	0.6693(7)	1	0.66(8)
X4a	O^{2-} / F^-	2*e*	0.0367(5)	¼	0.1218(10)	0.69(1)	1.17(12)
X4b	O^{2-} / F^-	2*e*	0.0689(12)	¼	0.248(2)	0.31(1)	1.17(12)
X5	O^{2-}	4*f*	0.6727(3)	-0.0035(6)	0.6753(4)	1	0.39(6)
X6	O^{2-}	4*f*	0.8425(2)	-0.0105(5)	0.3747(4)	1	0.60(5)

a [Å]	10.1097(7)	**b [Å]**	5.7123(4)	**c [Å]**	6.9816(5)	**β [°]**	93.071(2)
GOF (overall)	1.34	**R_{wp} (overall)**	2.21 %	**R_{bragg} (NPD, b6)**	1.32 %	**R_{bragg} (XRD)**	0.66 %

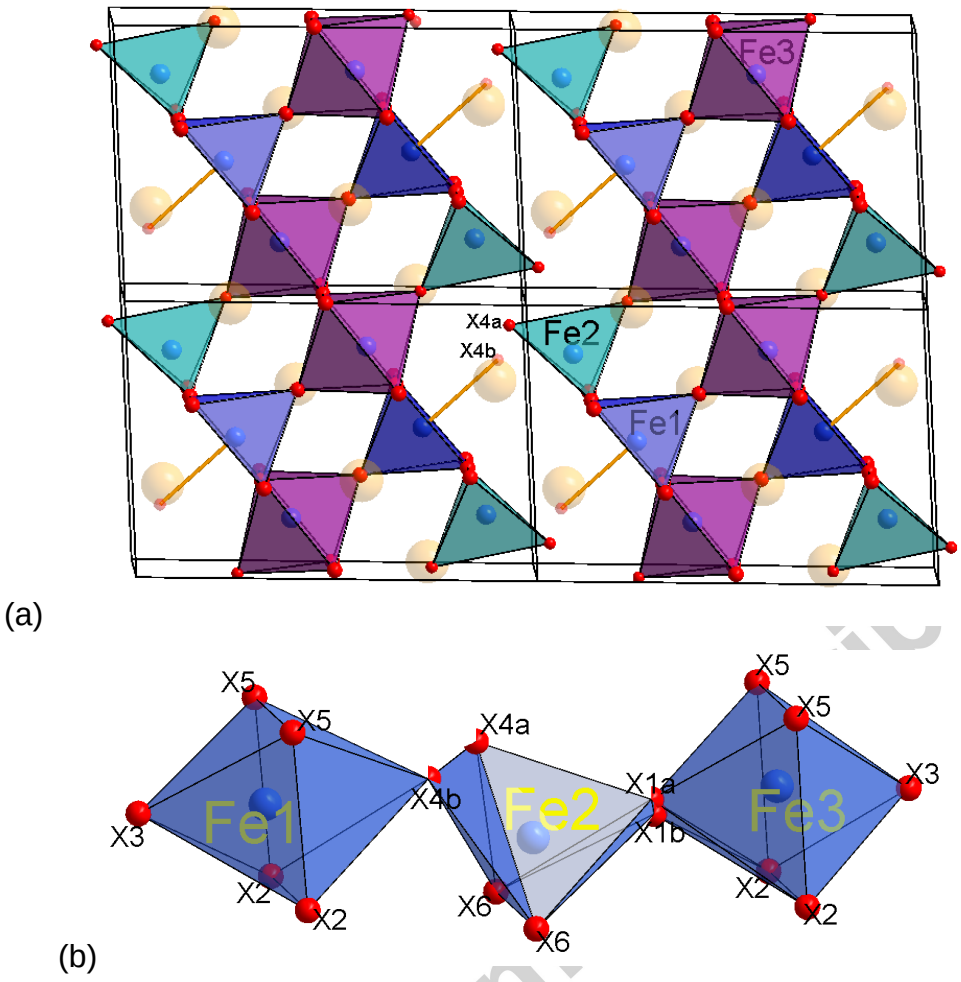

Figure 2. Refined crystal structure of $Ba_3Fe_3O_7F$ (a) together with an excerpt showing the detailed anion connectivity around the three different iron sites together with the interconnectivity (b).

Analysis of the data shows that the ordering pattern of anion vacancies of $Ba_3Fe_3O_7F$ as described previously in ref. [30] can be confirmed by means of neutron diffraction. Indeed, no indication even for partial occupation of the potential anion site 2*a* was given during the refinements. Therefore, this occupation factor was fixed to zero for the final analysis.

On analyzing the data further using anisotropic displacement parameters, we found that the thermal ellipsoids for the X1 and the X4 anion show a rod like shape, whereas all the other thermal ellipsoids of anions and cations appeared to be mainly spherical. This rod like shape cannot be considered to plausibly describe the thermal motion of those anions, but is more likely to result from a fluctuation of the detailed position of the anion in a partially disordered structure. Therefore, two independent anion sites X1a/b and X4a/b were used for both the X1 and X4 ions, for which positional parameters were refined independently. Indeed, a strong splitting of the

anion site was observed for the X4 anion (d(X4a-X4b) = 0.92(2) Å), whereas the splitting of the X1 ion was only moderate (d(X1a-X1b) = 0.23(7) Å). The use of split sites resulted in overall plausible isotropic displacement parameters, as shown in Table 1, to which our final model was limited. All anion-cation distances agree well with what is usually found for Fe^{3+} containing perovskite type oxides and oxyfluorides (see Table 2 for a list of Fe-X distances). In this respect it is worth pointing out that strong differences in the order of 0.1 – 0.2 Å can be found in comparison to our previous analysis, which was based on XRPD only, highlighting the impact on including neutron diffraction data for obtaining reliable bond distances for further analysis. Additionally, in our previous work it was also not possible to determine the split site feature from the analysis of XRD data only.

Table 2. Iron to anion distances found for $Ba_3Fe_3O_7F$.

Fe^{3+}-X bond distances [Å]					
Fe1, CN = 5		**Fe2, CN = 4**		**Fe3, CN = 6**	
1x X3	1.974(6)	1x X4a	1.762(6)	1x X1b	1.943(37)
2x X5	1.974(4)	2x X6	1.878(3)	1x X1a	1.958(54)
2x X6	1.988(3)	1x X4b	1.900(12)	2x X5	1.966(4)
1x X4b	2.547(13)	1x X1b	1.904(37)	1x X3	2.050(6)
1x X4a	3.379(7)	1x X1a	1.910(57)	2x X2	2.151(2)

Bond valence sums (BVSs) were then calculated for each anion to determine the most likely distribution of oxide and fluoride ions in the structure (see Table 3). To obtain a composition of $Ba_3Fe_3O_7F$, 2 of the 16 anions of the monoclinic unit cell must be fluoride ions. For complete anion ordering one would therefore expect one of the anion sites with 2-fold multiplicity to show a BVS of approximately 1, with all other anion sites showing a BVS of ~ 2. Contrary to this expectation, one finds that the X2 and X4a/b ions show significant deviation from a BVS sum of 2. However, neither of these two sites can be assigned to be fully occupied by a fluoride ion either. From the BVSs found, one could expect half occupation of each of these sites by both oxide and fluoride ions, as will be outlined in the following.

Table 3. Bond valence sums (BVSs) calculated for the different anion sites for $Ba_3Fe_3O_7F$ together with mutual assignment to the respective types of anions. The sums for X1a/b, X3, X5, and X6 were calculated with the BVS parameters for oxide ions, whereas for X2 and X4a/b the BVS parameters for oxide and fluoride were tested.

anion site	site multiplicity	BVS	assignment
X1a	2	2.00	Mainly O^{2-}
X1b		2.02	
X2	2	1.63 for X2 = O 1.32 for X2 = F	Presumably mixed occupation O^{2-} + F^-
X3	2	1.88	Mainly O^{2-}
X4a	2	1.69 for X4a = O 1. 38 for X4a = F	Presumably mixed occupation O^{2-} + F^-
X4b		1.46 for X4b = O 1.19 for X4b = F	
X5	4	1.92	Mainly O^{2-}
X6	4	1.88	Mainly O^{2-}

Special attention needs to be drawn to the split anion site X4a/X4b. Since the BVSs overall indicate a mixed occupation of the X4 site, one can easily imagine that one of the split positions might more likely represent the position of an oxide ion, whereas the other one more likely describes the location of the fluoride ion. In this respect, we find it noteworthy that the X4b site (which shows a weak additional bond to the Fe1 ion, see Figure 2) shows a significantly lower BVS than the X4a site (which shows a very short bond to Fe2 and a very long bond to Fe1). Therefore, the X4b site is more likely to represent the position of the fluoride ion. In addition, the X4a site shows similar behavior to what is found for fluorine free $Ba_2Fe_2O_5$ [33], for which also non-shared as well as weakly shared oxide ions are found for tetrahedrally coordinated iron species. Furthermore, it is interesting to compare $Ba_3Fe_3O_7F$ to the structurally similar compound $Ba_3Fe_3O_7(OH)$ [37]. For the latter, the tetrahedrally coordinated iron species are not connected to the hydroxide groups (which possess the same charge as a fluoride ion), but form an additional very short bond to a neighbouring Ba^{2+} ion (see Figure 3). Therefore, this represents a major difference comparing the structural chemistry of the hydroxide to the fluoride ion in a perovskite matrix. This difference probably results from the fact that the location of the proton of the hydroxide group might be in conflict with the relaxations of the A and B site cations around the tetrahedrally coordinated iron species. In contrast, the fluoride ion does not possess

a positive dipolar moment, for which strong repulsive interactions to surrounding cations would have to be expected.

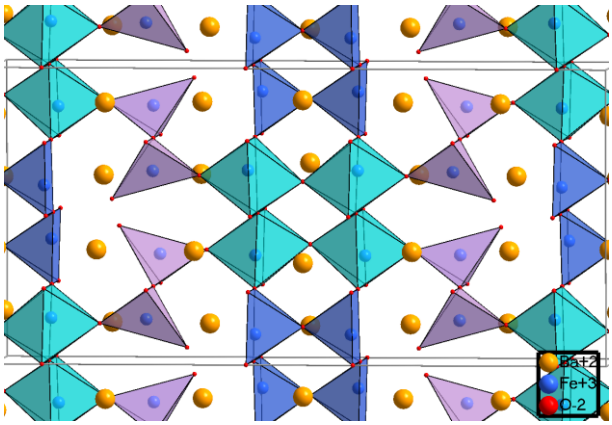

Figure 3. Structure excerpt of $Ba_3Fe_3O_7(OH)$ [37]. Different colours are shown for Fe^{3+} coordination polyhedra of different crystallographic Fe sites.

For 6H- and 15R-$BaFeO_2F$ [38], some of the iron ions are located between c-type layers of composition BaO_3 and h-type layers of composition BaF_3, resulting in octahedral coordination of Fe with opposite faces of the octahedron consisting of oxide and fluoride ions only. In those compounds, short bond Fe-O bond distances of ~ 1.85 Å and longer bond distances Fe-F of ~ 2.22 Å are found. This observation might appear to be counterintertuitive from the ionic radii of O^{2-} and F^- (which have been determined from oxide and fluoride compounds, not for oxyfluorides, with F^- being the smaller anion [1] in this very qualitative approach). However, one also needs to take into account the charge differences of O^{2-} and F^-, which should result in stronger attractive forces to the higher charged anion. This behaviour is also reflected in the bond distances of X4a and X4b, with X4a forming one very short and one very long bond (1.76 and 3.38 Å) and X4b forming a longer and one very long bond (1.90 and 2.55 Å). Therefore, the investigation of the bond distances gives further support for the mutual assignment of oxide and fluoride ions.

On a further note, the X1a/b anion site is most likely to be occupied by the oxide anion only. This is in agreement with the small difference in position of the two anions X1a and X1b. The site splitting seems to arise mainly from the tilting of the tetrahedron resulting from the occupation of the X4a/b position by either an oxide or a fluoride anion.

Overall we conclude that $Ba_3Fe_3O_7F$ must be considered to show at least partial ordering of the anions, making the compound the first anion and vacancy ordered oxyfluoride perovskite within a purely *ccp* type stacking of AX_{3-d} layers.

3.2 Magnetic Properties and Magnetic Structure of $Ba_3Fe_3O_7F$

A Field Sweep measurement (see Figure 4a) was performed at 300 and 5 K and indicates mainly antiferromagnetic behaviour of the compound, showing only a small ferromagnetic moment of approximately 0.0002 μ_B per Fe atom. FC / ZFC measurements (see Figure 4b) on $Ba_3Fe_3O_7F$ also agree with this antiferromagnetic behaviour of the compound, with the difference between the curves resulting from the presence of the small ferromagnetic component. This ferromagnetic contribution could be explained from (a) either a small canting moment (see comment later in this section) or (b) the presence of a small impurity phase undetectable by means of powder diffraction techniques. Those findings are very similar to other $BaFeO_2F$ / $BaFeO_{2.5}$ compounds previously reported [17, 19, 33, 38, 39].

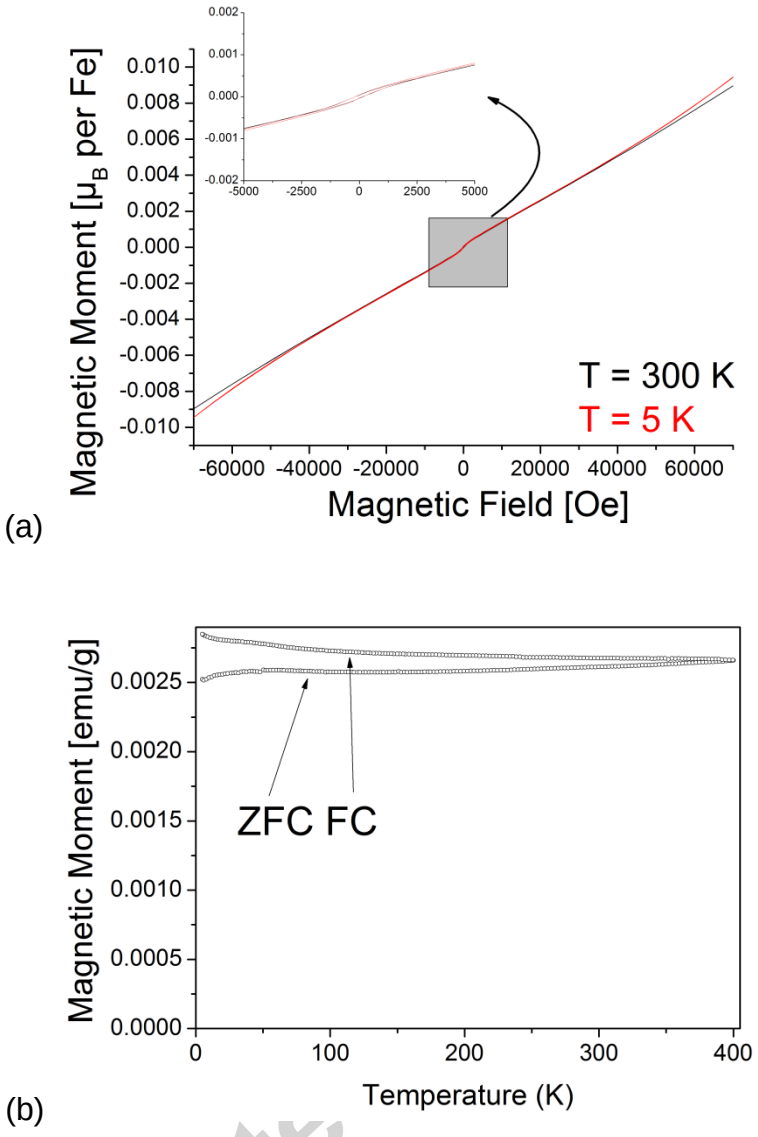

Figure 4. Field Sweep (a) as well as FC/ZFC measurements (b) on $Ba_3Fe_3O_7F$.

As can be seen in Figure 1, additional reflections arising from magnetic scattering can be found in the neutron diffraction patterns at ambient temperature. Those reflections can be well indexed using a unit cell with $a_{mag} = a_{nuc}$, $b_{mag} = b_{nuc}$ and $c_{mag} = 2*c_{nuc}$, corresponding to a magnetic k-vector of [0 0 ½]. Furthermore, the main d-spacing values of the magnetic reflections coincide with what we previously found for perovskite type ferrites with *ccp* type stacking of AX_3 layers, which show G-type antiferromagnetic alignment of magnetic moments [19, 33]. Using the tools provided on the Bilbao Crystallographic Server [40-43], we found that there are two different maximal magnetic subgroups of $P2_1/m$. Those are the magnetic space groups (BNS notation) 14.82 and 11.55, with two different settings for each space group. Those settings distinguish with respect to the choice of the origin (0, 0, 0 and 0, 0, ½). Therefore, possible maximal magnetic symmetries compatible with k = [0 0 ½] differ with regards

to the location of the centres of inversion which are being maintained on breaking of the nuclear symmetry. We would like to comment to the reader that the restrictions of the magnetic vectors for the magnetic space groups 14.82 with the two different choices of origin correspond to the irreducible representations Γ_1 and Γ_4, whereas the restrictions for 11.55 belong to the irreducible representation Γ_2 and Γ_3.

Magnetic structural models were constructed for each of the four possible settings with maximal magnetic symmetry. Rietveld analysis showed that reasonable fits to the observed magnetic intensities can only be obtained for space group 11.55 with a shift of origin of 0, 0, ½ (in relation to the crystallographic structure as described in Table 1). This symmetry corresponds to a G-type antiferromagnetic arrangement of the magnetic moments (see Figure 5 for a plot of the magnetic structure) at ambient temperature. For this magnetic symmetry, the magnetic vectors are restricted to align parallel to the nuclear b-axis, with components of the magnetic vector along the nuclear a- and c-axes being restricted to be 0. This is also the main difference from the space group 14.82 which restricts the magnetic vector to align within the ac-plane (although showing G-type order at the same time). This alternative orientation of the magnetic vector does not reproduce the observed magnetic scattering contribution to the neutron diffraction pattern and can therefore be discounted.

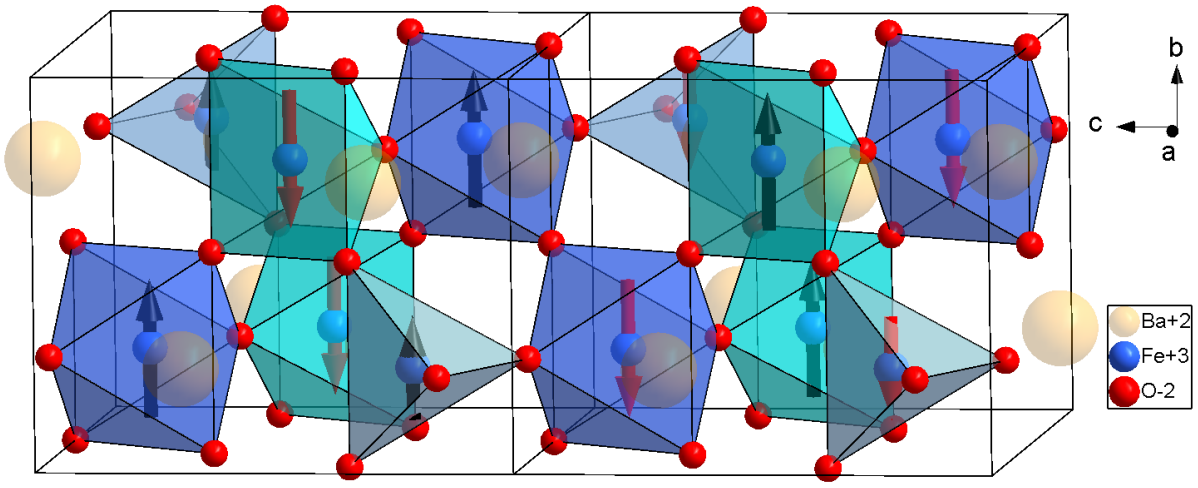

Figure 5. Magnetic structure of $Ba_3Fe_3O_7F$ (no split sites and potential O/F ordering shown) with relation to the nuclear unit cell showing doubling of the c-axis for the magnetic cell (k-vector [0 0 ½]).

In relation to an analysis with the programs BasIreps available in the FullProf suite [44] or ISODISTORT [45], we performed an analysis of possible irreducible representations for the atoms located on the 2e site in space group $P2_1/m$ with a magnetic propagation vector k = [0 0 ½]. The restrictions of the magnetic vectors for the

magnetic space groups 14.82 with the two different choices of origin correspond to the vector transformations according to the irreducible representations mGm1- and mGm2+, whereas the restrictions for the space groups 11.55 (again with the two different choices of origin) correspond to the vector transformations according to the irreducible representation mGm1+ and mGm2-. The magnetic moments of the Fe atoms in $Ba_3Fe_3O_7F$ are found to transform according to the irreducible representation mGm1+.

Magnitudes of magnetic vectors as obtained from the refinement are listed in Table 4 and agree very well with what would be expected from iron in a trivalent high-spin state. The overall magnitude of the moments is similar to what was found for similar compounds [19, 33]. In agreement with our previous findings on $BaFeO_{2.5}$ and values for magnetic hyperfine field splitting of $Ba_3Fe_3O_7F$ determined by means of Mössbauer spectroscopy in ref. [30], the magnitude of the magnetic vector is slightly reduced whenever the iron ion is found in a tetrahedral coordination. This can be explained by increased covalent bonding for smaller coordination numbers. Although small ferrimagnetic moments are formed locally (e. g. for connected Fe1(up)-O-Fe2(down)), the magnetic symmetry of the magnetic space group 11.55 causes a cancelling of such local ferrimagnetic moments, being in agreement with the overall antiferromagnetic properties of $Ba_3Fe_3O_7F$. In this respect, it is also worth noting that the magnetic space group 11.55 does not permit for the presence of a small canting moment. Therefore, the small magnetic moment which was observed by means of SQUID magnetometry could either be explained from further symmetry lowering (disorder which breaks the local symmetry, i. e. local small differences in J parameters due to the partially disordered anion sublattice) or from the presence of a small amount of impurity phase such as e. g. $BaFe_{12}O_{19}$ [46] (with the latter not being indicated from the analysis of diffraction data). However, we would like to acknowledge that an unambiguous determination of such small canting moments is not possible by means of powder neutron diffraction due to the limited amount of magnetic reflections and the very small magnitude of the canting moment itself.

Table 4. Magnetic moments as determined by means of neutron powder diffraction at ambient temperature in comparison to magnetic hyperfine fields as determined by Mössbauer Spectroscopy [30].

site	Coordination Number	Magnitude of Magnetic Moment as determined by neutron powder diffraction [μ_B]	B_{hf} from the analysis of Mössbauer data [T] [30]
Fe1	5	3.7(1)	49.1(5)
Fe2	4	3.5(1)	42.0(1)
Fe3	6	3.8(1)	50.6(5)

The orders of magnetic moments found for $Ba_3Fe_3O_7F$ at ambient temperature are very similar to what is found for other compounds (e. g. the three different modifications of $BaFeO_2F$), which have Néel temperatures between 597 – 645 K and are robust antiferromagnets [47]. Therefore, we assume that the magnetic ordering temperature of $Ba_3Fe_3O_7F$ can be expected to be in the same order of magnitude, since the type of superexchange interactions (~180° AFM d^5-d^5) are promoted by the same type of anions with similar Fe-(O/F)-Fe bond angles.

4 Conclusions

$Ba_3Fe_3O_7F$ is the first compound showing both, ordering of anion vacancies in addition to partial ordering of oxide and fluoride ions within a *ccp* related stacking of AX_3 layers within a perovskite type structure. This highlights the potential impact of strong structural distortions resulting from anion ordering on establishing different anion site potentials within a perovskite matrix. In addition, the ordering of anion seems to have little impact on the principal G-type antiferromagnetic arrangement of magnetic moments, which is facilitated by strong antiferromagnetic superexchange interactions between corner shared polyhedra of high spin Fe^{3+} with d^5 electronic configuration (Fe-X-Fe bond angles approaching 180°).

Acknowledgements

O. Clemens gratefully acknowledges support from the German Research Foundation (Deutsche Forschungsgemeinschaft, DFG) within an Emmy Noether Research Fellowship (grant no. CL551/2-1). Xpress Access neutron beamtime on GEM at ISIS was provided by the Science and Technology Facilities Council (STFC).

References

1. R. D. Shannon, *Acta Crystallogr.*, 1976, A32, 751-767.
2. M. Leblanc, V. Maisonneuve and A. Tressaud, *Chem. Rev. (Washington, DC, U. S.)*, 2015, 115, 1191-1254.
3. P. R. Slater, *J. Fluorine Chem.*, 2002, 117, 43-45.
4. C. Greaves and M. G. Francesconi, *Curr. Opin. Solid State Mater. Sci.*, 1998, 3, 132-136.
5. E. E. McCabe and C. Greaves, *J. Fluorine Chem.*, 2007, 128, 448-458.
6. O. Clemens and P. R. Slater, *Rev. Inorg. Chem.*, 2013, 33, 105-117.
7. G. Ehora, C. Renard, S. Daviero-Minaud and O. Mentré, *Chem. Mater.*, 2007, 19, 2924-2926.
8. O. Mentré, H. Kabbour, G. Ehora, G. g. Tricot, S. Daviero-Minaud and M.-H. Whangbo, *J. Am. Chem. Soc.*, 2010, 132, 4865-4875.
9. M. Sturza, S. Daviero-Minaud, H. Kabbour, O. Gardoll and O. Mentré, *Chem. Mater.*, 2010, 22, 6726-6735.
10. M. Sturza, H. Kabbour, S. Daviero-Minaud, D. Filimonov, K. Pokholok, N. Tiercelin, F. Porcher, L. Aldon and O. Mentré, *J. Am. Chem. Soc.*, 2011, 133, 10901-10909.
11. M. Iorgulescu, P. Roussel, N. Tancret, N. Renault, F. Porcher, G. André, H. Kabbour and O. Mentré, *Inorg. Chem.*, 2012, 51, 7598-7608.
12. I. D. Brown, *The chemical bond in inorganic chemistry: the bond valence model*, Oxford University Press Inc., New York, 2002.
13. L. D. Aikens, R. K. Li and C. Greaves, *Chem. Commun. (Cambridge, U. K.)*, 2000, 2129-2130.
14. M. V. Lobanov, A. M. Abakumov, A. V. Sidorova, M. G. Rozova, O. G. D'Yachenko, E. V. Antipov, J. Hadermann and G. Van Tendeloo, *Solid State Sci.*, 2002, 4, 19-22.
15. A. M. Alekseeva, A. M. Abakumov, M. G. Rozova, E. V. Antipov and J. Hadermann, *J. Solid State Chem.*, 2004, 177, 731-738.
16. E. V. Antipov, A. M. Abakumov, A. M. Alekseeva, M. G. Rozova, J. Hadermann, O. I. Lebedev and G. Van Tendeloo, *Phys. Status Solidi A*, 2004, 1, 1403-1409.
17. R. Heap, P. R. Slater, F. J. Berry, O. Helgason and A. J. Wright, *Solid State Commun.*, 2007, 141, 467-470.
18. O. Clemens, R. Haberkorn, P. R. Slater and H. P. Beck, *Solid State Sci.*, 2010, 12, 1455-1463.
19. F. J. Berry, F. C. Coomer, C. Hancock, Ö. Helgason, E. A. Moore, P. R. Slater, A. J. Wright and M. F. Thomas, *J. Solid State Chem.*, 2011, 184, 1361-1366.
20. F. J. Berry, X. Ren, R. Heap, P. Slater and M. F. Thomas, *Solid State Commun.*, 2005, 134, 621-624.
21. F. J. Berry, R. Heap, Ö. Helgason, E. A. Moore, S. Shim, P. R. Slater and M. F. Thomas, *J. Phys.: Condens. Matter*, 2008, 20, 215207.
22. C. K. Blakely, J. D. Davis, S. R. Bruno, S. K. Kraemer, M. Zhu, X. Ke, W. Bi, E. E. Alp and V. V. Poltavets, *J. Fluorine Chem.*, 2014, 159, 8-14.
23. C. M. Thompson, C. K. Blakely, R. Flacau, J. E. Greedan and V. V. Poltavets, *J. Solid State Chem.*, 2014, 219, 173-178.
24. O. Clemens, F. J. Berry, A. J. Wright, K. S. Knight, J. M. Perez-Mato, J. M. Igartua and P. R. Slater, *J. Solid State Chem.*, 2015, 226, 326-331.
25. C. M. Thompson, C. K. Blakely, R. Flacau, J. E. Greedan and V. V. Poltavets, *J. Solid State Chem.*, 2015, 226, 332-333.

26. Y. Inaguma, J.-M. Greneche, M.-P. Crosnier-Lopez, T. Katsumata, Y. Calage and J.-L. Fourquet, *Chem. Mater.*, 2005, 17, 1386-1390.
27. T. Katsumata, H. Umemoto, Y. Inaguma, D. Fu and M. Itoh, *J. Appl. Phys.*, 2008, 104, 044101.
28. W. Rüdorff and D. Krug, *Z. Anorg. Allg. Chem.*, 1964, 329, 211-217.
29. M. T. Anderson, J. T. Vaughey and K. R. Poeppelmeier, *Chem. Mater.*, 1993, 5, 151-165.
30. O. Clemens, *J. Solid State Chem.*, 2015, 225, 261-270.
31. M. Parras, L. Fournes, J. C. Grenier, M. Pouchard, M. Vallet, J. M. Calbet and P. Hagenmuller, *J. Solid State Chem.*, 1990, 88, 261-268.
32. X. D. Zou, S. Hovmoller, M. Parras, J. M. Gonzalez-Calbet, M. Vallet-Regi and J. C. Grenier, *Acta Crystallogr.*, 1993, A49, 27-35.
33. O. Clemens, M. Groeting, R. Witte, J. Manuel Perez-Mato, C. Loho, F. J. Berry, R. Kruk, K. S. Knight, A. J. Wright, H. Hahn and P. R. Slater, *Inorg. Chem.*, 2014, 53, 5911-5921.
34. *Topas V4.2, General profile and structure analysis software for powder diffraction data, User's Manual*, Bruker AXS, Karlsruhe, Germany, 2008.
35. A. A. Coelho, TOPAS-Academic, http://www.topas-academic.net, Accessed 20th of October 2014.
36. R. W. Cheary, A. A. Coelho and J. P. Cline, *J. Res. Nat. Inst. Stand. Technol.*, 2004, 109, 1-25.
37. P. L. Knöchel, P. J. Keenan, C. Loho, C. Reitz, R. Witte, K. S. Knight, A. J. Wright, H. Hahn, P. R. Slater and O. Clemens, *J. Mater. Chem. A*, 2016, 4, 3415-3430.
38. O. Clemens, F. J. Berry, J. Bauer, A. J. Wright, K. S. Knight and P. R. Slater, *J. Solid State Chem.*, 2013, 203, 218-226.
39. O. Clemens, A. J. Wright, F. J. Berry, R. I. Smith and P. R. Slater, *J. Solid State Chem.*, 2013, 198, 262-269.
40. MGENPOS in the Bilbao Crystallographic Server, http://cryst.ehu.es, Accessed 20th of October 2014.
41. MAXMAGN in the Bilbao Crystallographic Server, http://cryst.ehu.es, Accessed 20th of October 2014.
42. M. I. Aroyo, A. Kirov, C. Capillas, J. M. Perez-Mato and H. Wondratschek, *Acta Crystallogr.*, 2006, A62, 115-128.
43. M. I. Aroyo, J. M. Perez-Mato, C. Capillas, E. Kroumova, S. Ivantchev, G. Madariaga, A. Kirov and H. Wondratschek, *Z. Kristallogr.*, 2006, 221, 15-27.
44. J. Rodriguez-Carvajal, *Physica B: Condensed Matter*, 1993, 192, 55-69.
45. B. J. Campbell, H. T. Stokes, D. E. Tanner and D. M. Hatch, *J. Appl. Crystallogr.*, 2006, 39, 607-614.
46. O. Clemens, R. Kruk, E. A. Patterson, C. Loho, C. Reitz, A. J. Wright, K. S. Knight, H. Hahn and P. R. Slater, *Inorg. Chem.*, 2014, 53, 12572-12583.
47. O. Clemens, J. F. Marco, M. F. Thomas, S. D. Forder, H. Zhang, S. Cartenet, A. Monze, P. Bingham, P. R. Slater and F. J. Berry, *Journal of Physics Condensed Matter*, 2016, 28, 346001.

Figure Captions

Figure 1. Combined Rietveld analysis of XRPD and NPD data recorded on the sample with composition $Ba_3Fe_3O_7F$. Partial fit curves are shown for nuclear phases (monoclinic $Ba_3Fe_3O_7F$ and cubic $BaFeO_{2+x}F_{1-2x}$) as well as for the magnetic scattering observed from $Ba_3Fe_3O_7F$ (see section 3.2).

Figure 2. Refined crystal structure of $Ba_3Fe_3O_7F$ (a) together with an excerpt showing the detailed anion connectivity around the three different iron sites together with the interconnectivity (b).

Figure 3. Structure excerpt of $Ba_3Fe_3O_7(OH)$ [37]. Different colours are shown for Fe^{3+} coordination polyhedra of different crystallographic Fe sites.

Figure 4. Field Sweep (a) as well as FC/ZFC measurements (b) on $Ba_3Fe_3O_7F$.

Figure 5. Magnetic structure of $Ba_3Fe_3O_7F$ (no split sites and potential O/F ordering shown) with relation to the nuclear unit cell showing doubling of the c-axis for the magnetic cell (k-vector [0 0 ½]).

Highlights

- $Ba_3Fe_3O_7F$ possesses a unique vacancy order not found for other perovskite type compounds.
- The valence bond method was used to locate oxide and fluoride ions.
- Fluoride ions are distributed only on two of the six anion sites in $Ba_3Fe_3O_7F$.
- The compound shows G-type antiferromagnetic ordering of magnetic moments.
- The magnetic structure could be refined in one of the maximal magnetic subgroups of the nuclear structure.